IEEE Access
Multidisciplinary | Rapid Review | Open Access Journal

Received October 9, 2020, accepted November 2, 2020, date of publication November 9, 2020, date of current version November 19, 2020.

Digital Object Identifier 10.1109/ACCESS.2020.3036866

Compact Low-Loss Electroabsorption Modulator Using a Graphene-Inserted Metal-Slot-Added Waveguide

JIHOON SEO AND MIN-SUK KWON

Department of Electrical and Computer Engineering, Ulsan National Institute of Science and Technology, Ulsan 44919, South Korea

Corresponding author: Min-Suk Kwon (mskwon@unist.ac.kr)

This work was supported by the Samsung Research Funding and Incubation Center for Future Technology under Grant SRFC-IT1901-07.

ABSTRACT Metal slots have been used to obtain strong light-graphene interaction, which usually requires them to be a few tens of nanometers wide. However, narrow metal slot waveguides have a large intrinsic loss; they are not efficiently connected to conventional silicon photonic waveguides; they are not easy to fabricate. To address the issues, a graphene-inserted metal-slot-added (GIMSA) waveguide and an electroabsorption modulator (EAM) based on it are theoretically investigated. The GIMSA waveguide consists of a silicon strip embedded in silicon dioxide and a metal slot aligned above the silicon strip with double graphene layers between them. The EAM is composed of the GIMSA waveguide and input and output couplers connecting it to silicon photonic waveguides. In order to achieve the good performance of the EAM in terms of length and insertion loss, the GIMSA waveguide and the couplers are designed. When the silicon strip and the metal slot are respectively 320 nm and 316 nm wide, the total length of the EAM with an extinction ratio of 3 dB is 6.23 μm, and its on-state insertion loss is 1.01 dB. Compared to previous graphene-based EAMs embedded in silicon photonic integrated circuits, this EAM is shorter and has a quite small insertion loss. The EAM's large feature size may enable fabrication using 248 nm optical lithography, and the EAM is expected to function as a compact modulator, well-integrated with silicon photonic devices.

INDEX TERMS Integrated optics, intensity modulation, nanophotonics, optical waveguides, silicon photonics, graphene.

I. INTRODUCTION

Since graphene emerged as a wonder material, it has led to the development of diverse photonic and plasmonic devices with unprecedented features enabled by its extraordinary optical properties like its electrically tunable optical conductivity [1]–[3]. Graphene-based waveguide modulators are a representative example of such devices, and a lot of effort has been devoted to inventing more compact modulators operating faster [4]–[8]. The essence of the invention is to devise waveguide structures with as strong light-graphene interaction as possible. Strong light-graphene interaction can be achieved when graphene is located at the position where the in-plane electric field component of a waveguide mode is highly enhanced. A few examples of such waveguide structures, which have been experimentally investigated, are a silicon (Si) slot waveguide [9], a photonic crystal waveguide [10], [11], a hybrid plasmonic waveguide [12]–[14], etc. In addition to them, various nanoplasmonic waveguides mainly focusing on a larger modulation depth have been theoretically studied [15]–[22].

Among a variety of graphene-based waveguides, metal slot waveguides covered with graphene are an attractive structure since the smaller the dimensions of the metal slots are, the stronger electric field the waveguides confine within the slots [23]–[25]. Recently, a bilayer-graphene-covered metal slot waveguide with dimensions of 30 nm $\times$ 20 nm was realized to demonstrate that it has a record-high modulation depth of 0.7 dB/μm when it is optically modulated by a femtosecond pulse of energy 20 fJ [25]. However, the strong light-graphene interaction of metal slot waveguides is obtained at the cost of a precise fabrication process based on electron-beam lithography. In addition, metal slot waveguides have a larger loss as their sizes decrease. Moreover, the coupling between a metal slot waveguide and a conventional Si strip waveguide is not generally efficient: the coupling loss in most realized devices is larger than 1 dB (*e.g.*, 1.7 dB in [25] and 1.45 dB in [24]). Therefore, it is

The associate editor coordinating the review of this manuscript and approving it for publication was Wei E. I. Sha.

required to develop a low-loss graphene-based waveguide using a metal slot, which retains strong light-graphene interaction but can be realized by using deep UV lithography as well as coupled efficiently to a Si strip waveguide.

In this paper, we theoretically investigate an electroabsorption modulator (EAM) based on a graphene-inserted metal-slot-added (GIMSA) waveguide. The metal slot of the GIMSA waveguide is placed above a Si strip with double graphene layers between them. The graphene layers interact with the strong electric field confined in the thin region between the metal slot and the Si strip. We show that the GIMSA waveguide has a large modulation depth of $\sim$0.73 dB/μm and a small insertion loss of $\sim$0.19 dB/μm whereas the metal slot and the Si strip have sizes large enough to be obtained from 248 nm optical lithography. We also show that the coupling loss between the GIMSA waveguide and a conventional Si strip waveguide can be reduced to the level of 0.1 dB. When the metal slot is 316 nm wide, the EAM with an extinction ratio of 3 dB is demonstrated to have the best performance: the product of the total length and total insertion loss of the EAM becomes minimum (the total length is 6.23 μm, and the total insertion loss is 1.01 dB). Contradictory to the idea that narrow metal slots may be better for graphene-based modulation, the result indicates that the wide metal slot is better for the EAM performance. Recently, a waveguide similar to the GIMSA waveguide has been studied [26]. Compared to the study, we focus on not just the GIMSA waveguide but rather the EAM and study in more depth the characteristics of the GIMSA waveguide over broader ranges of structural parameters. We expect that the EAM based on the GIMSA waveguide may function as a compact low-loss modulator well embedded in Si photonic integrated circuits, which is practically realizable with 248 nm optical lithography.

II. STRUCTURE AND MODE CHARACTERISTICS

The modulator investigated in this work consists of the GIMSA waveguide and two input and output couplers which connect the GIMSA waveguide and conventional Si waveguides. It is schematically shown in Fig. 1(a) and (b). The input coupler converts the fundamental transverse-electric (TE) mode of the Si photonic waveguide to the mode of the GIMSA waveguide; the mode power is modulated by the strong light-graphene interaction existing in the GIMSA waveguide; the output coupler converts back the mode to the fundamental TE mode. As shown in Fig. 1(c), the GIMSA waveguide is comprised of the Si strip embedded in silicon dioxide (SiO_2), the graphene-aluminum oxide (Al_2O_3)-graphene capacitor, and the metal slot made of gold aligned to the center of the Si strip. The height of the Si strip is set at 250 nm, and the thickness of the Al_2O_3 layer is set at 10 nm. The width of the Si strip is denoted by w_s, and the width and height of the metal slot are denoted by w_m and h_m, respectively. The graphene layers overlap in a finite region of width w_o; the metal rail, which forms the metal slot in company with electrode 2, has a width of w_r; the spacing

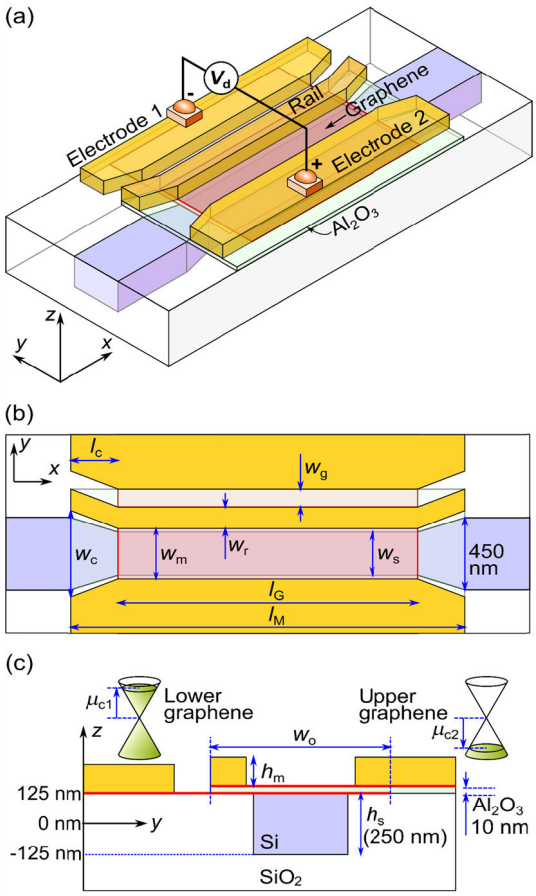

FIGURE 1. Structure of the EAM. (a) Perspective view of the EAM. (b) Top view of the EAM. The GIMSA waveguide is connected to the input and output Si waveguides via the couplers. The metal slot, aligned to the Si strip, is formed by the metal rail of width w_r and electrode 2. The width of the metal slot is w_m, and that of the Si strip is w_s. In the coupler, w_m and w_s increases to w_c and 450 nm, respectively, over a distance l_c. (c) Cross-sectional structure of the GIMSA waveguide. The height of the metal slot is h_m, and that of the Si strip is h_s. h_s is set at 250 nm, and the thickness of the Al_2O_3 layer is set at 10 nm. It is assumed that the chemical potential of the graphene connected to electrode 1 (2) is μ_{c1} (μ_{c2}) and $\mu_{c1} = -\mu_{c2}$.

between the metal rail and electrode 1 is denoted by w_g. Electrodes 1 and 2 control the chemical potentials μ_{c1} and μ_{c2} of the lower and upper graphene layers. Since electrode 2 functions as a part of the metal slot as well as an electrode, the whole metal structure is simpler than that in [26]. w_o and w_r are made large enough not to affect the characteristics of the GIMSA waveguide as discussed below. The coupler is the region of length l_c where the Si strip width linearly increases from w_s to 450 nm (the strip width of the Si photonic waveguide) and the metal slot width also linearly increases from w_m to w_c.

Before designing the modulator, it is important to look into the mode characteristics of the GIMSA waveguide. To analyze the GIMSA waveguide, we used an eigenmode solver based on the finite difference method (MODE, Lumerical Inc.). The refractive indices of Si, SiO_2, Al_2O_3 and gold are 3.45, 1.44, 1.74, $0.559 + i9.81$, respectively, at a wavelength of 1550 nm. Graphene was treated as a conducting boundary with an optical conductivity σ_g. For σ_g, an analytic expression

derived from the Kubo formula [27] was used with the relaxation time of graphene set at 0.1 ps. For various values of w_m and w_s, we determined the GIMSA waveguide mode, which is dominantly polarized in the y direction, under the assumption that w_o and w_r are infinite and $h_m = 150$ nm. It is the only TE mode guided by the GIMSA waveguide with $w_s \leq 450$ nm. We normalized the electric and magnetic fields of the mode such that the power carried by the mode is 1 mW. Since the graphene layers interact with the in-plane component E_y of the electric field $\mathbf{E}$, it is necessary to check how large portion of E_y exists at the positions of the graphene layers. For this purpose, we defined a factor of confinement of E_y per unit length, $\Gamma(z)$ as

$$\Gamma(z) = \int_{L_z} |E_y|^2 \, dy \Big/ \int_{A_\infty} |\mathbf{E}|^2 \, dydz, \tag{1}$$

where L_z denotes the horizontal line at z and A_∞ represents the infinite cross-section of the waveguide. We calculated $\Gamma(z)$ for the various values of w_m and w_s.

The profiles of the mode electric field (in log scale) are shown in Fig. 2(a) to (c), and the curves of $\Gamma(z)$ are compared in Fig. 2(d) to (f). Unless either w_m or w_s is large, the electric field is mainly confined in the metal slot and it is strongly enhanced in the regions between the metal slot corners and the Si strip corners (it also exists within the skin depth from the metal surface, but it is very weak). The strong enhancement can be confirmed from the peaks of $\Gamma(z)$ at the graphene positions, which enable the GIMSA waveguide to have the strong light-graphene interaction. In the case of a Si strip waveguide embedded in SiO_2, its fundamental TE mode is supported at a wavelength of 1550 nm when the Si strip width is larger than 210 nm. Therefore, for $w_s = 150$ nm (Fig. 2(a)), the metal slot plays the key role in guiding the GIMSA waveguide mode. As w_m increases, the electric field confined in the metal slot becomes weaker, and $\Gamma(z)$ decreases as shown in Fig. 2(d). When $w_s = 320$ nm (Fig. 2(b)), a larger portion of the electric field is confined in the Si strip for a larger value of w_m. This matches the increase of $\Gamma(z)$ in the range corresponding to the Si strip ($-0.125\ \mu m < z < 0.125\ \mu m$), which is shown in Fig. 2(e). However, $\Gamma(z)$ at the graphene positions is still much larger than in the range of the Si strip when $w_m \leq w_s$. If $w_s = 450$ nm (Fig. 2(c)), the Si strip dominantly guides the GIMSA waveguide mode unless w_m is quite small (*e.g.*, 220 nm). As shown in Fig. 2(f), $\Gamma(z)$ in the range of the Si strip is significant as compared to $\Gamma(z)$ at the graphene positions when $w_m = w_s$. Interestingly, regardless of w_s, $\Gamma(z)$ has two peaks at the graphene positions if $w_m = w_s$. For $w_s = 150$ nm or 320 nm, $\Gamma(z)$ is very large at those positions. However, for $w_s = 450$ nm, the two peaks are just comparable to the values in the range of the Si strip. Consequently, the light-graphene interaction in the GIMSA waveguide becomes very strong if $w_m = w_s$ for $w_s = 150$ nm or 320 nm. In contrast, in the case of $w_s = 450$ nm, $w_m = 220$ nm results in the strongest light-graphene interaction. The results mean that there are two different ways of choosing w_m depending on w_s as shown below.

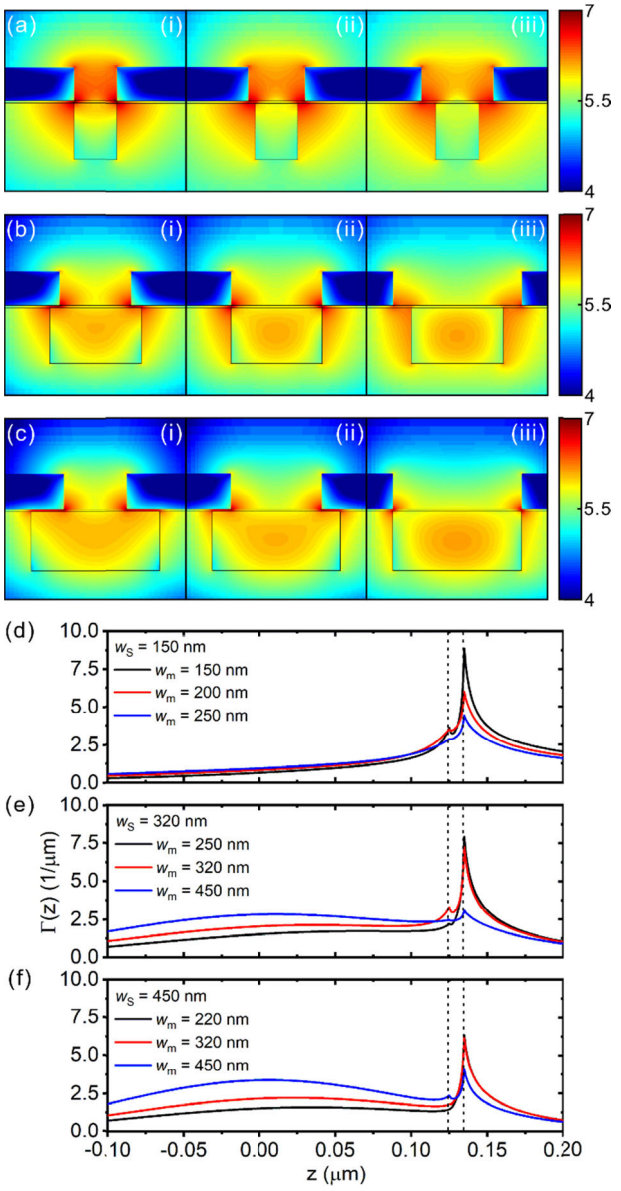

FIGURE 2. GIMSA waveguide mode at a wavelength of 1550 nm. Electric field distributions of the GIMSA waveguide mode for (a) $w_s = 150$ nm, (b) $w_s = 320$ nm, and (c) $w_s = 450$ nm. The distributions of $\log_{10}|E|$ are shown. In panel (a), w_m is equal to (i) 150 nm, (ii) 200 nm, and (iii) 250 nm. In panel (b), w_m is equal to (i) 250 nm, (ii) 320 nm, and (iii) 450 nm. In panel (c), w_m is equal to (i) 220 nm, (ii) 320 nm, and (iii) 450 nm. Relations between the factor of confinement, $\Gamma(z)$ and the vertical position (z) for (d) $w_s = 150$ nm, (e) $w_s = 320$ nm, and (f) $w_s = 450$ nm. The vertical dashed lines indicate the graphene positions.

III. MODULATOR DESIGN AND CHARACTERISTICS

A. DESIGN OF THE GIMSA WAVEGUIDE

The output power of the modulator is controlled by adjusting the voltage applied between electrodes 1 and 2. It is high (low) when the modulator is in the on-state (off-state) defined as the condition where $\mu_{c1} = -\mu_{c2} = 0.6$ eV (0.2 eV). The modulation depth of the GIMSA waveguide, denoted by MD_G, is defined as the difference between the off-state and on-state propagation losses (in dB/μm); the insertion loss of the GIMSA waveguide, denoted by IL_G, is defined

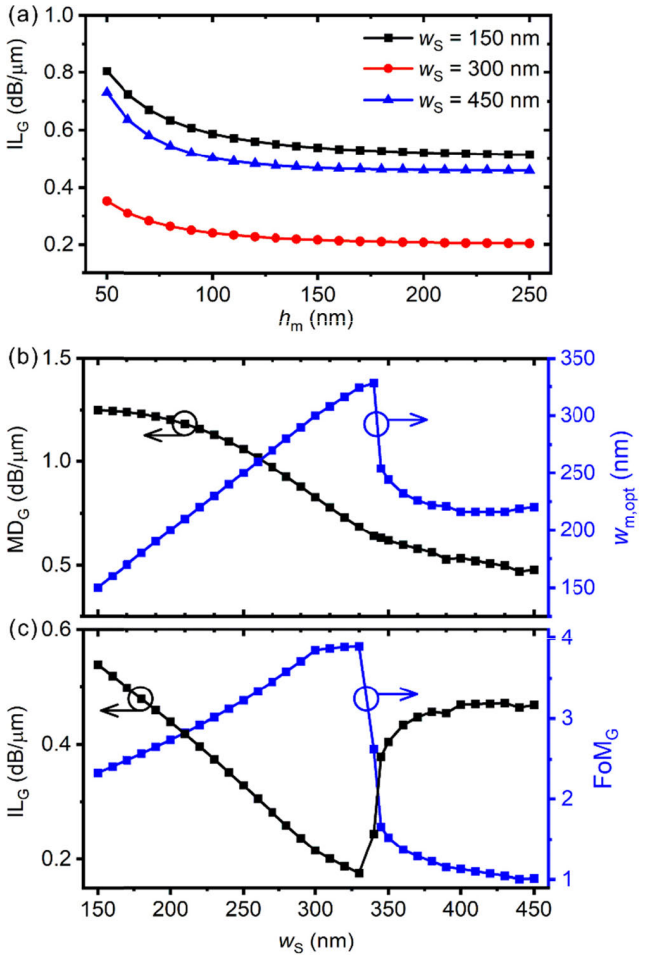

FIGURE 3. Dependence of the modulation depth (MD_G) and insertion loss (IL_G) of the GIMSA waveguide on the structural parameters at a wavelength of 1550 nm. (a) Relations of the IL_G to h_m for w_s = 150 nm, 300 nm, and 450 nm. (b) Relation of the optimal metal slot width $w_{m,opt}$ to w_s and relation of the MD_G, calculated for $w_m = w_{m,opt}$, to w_s. (c) Relation of the IL_G to w_s and relation of the figure of merit (FoM_G), defined as the ratio of the MD_G to the IL_G, to w_s. Both were calculated for $w_m = w_{m,opt}$.

as the on-state propagation loss. The design of the GIMSA waveguide is determining the values of w_s, w_m, and h_m such that the MD_G is maximized and the IL_G is minimized. For that purpose, we calculated the MD_G and the IL_G while changing the values of w_s, w_m, and h_m.

The relations of the IL_G to h_m are shown in Fig. 3(a) for (w_s, w_m) = (150 nm, 150 nm), (300 nm, 300 nm), and (450 nm, 220 nm). As h_m increases, the IL_G decreases and seems to approach a constant value for $h_m > 150$ nm. If h_m is small, the electric field of the GIMSA waveguide mode spills out to the top surface of the metal slot, and not only the bottom corners of the metal slot but also the top corners affect the mode. This makes the IL_G large. If h_m is sufficiently large, the electric field is well confined in the lower region of the metal slot, and the IL_G is almost independent of h_m. In order to minimize the influence of h_m and reduce the IL_G, we determined the value of h_m to be 150 nm.

Next, for a value of w_s, varying w_m, we calculated the MD_G and determined the optimal value of w_m, denoted by $w_{m,opt}$, which makes the MD_G maximum. $w_{m,opt}$ is shown as a function of w_s in Fig. 3(b). If $w_s \leq 300$ nm, $w_{m,opt} = w_s$. If w_s is between 300 nm and 340 nm, $w_{m,opt}$ is slightly smaller than w_s. For example, $w_{m,opt} = 328$ nm for $w_s = 340$ nm. Surprisingly, $w_{m,opt}$ decreases abruptly for w_s between 340 nm and 380 nm and it barely changes around 220 nm for $w_s > 380$ nm. As shown in Fig. 2(d) to (f), if $w_s \leq 340$ nm and $w_m \cong w_s$, $\Gamma(z)$ has the two strong peaks at the graphene positions, which make the MD_G maximized. However, for $w_s > 340$ nm, $\Gamma(z)$ has the dominant peak at the upper graphene position when $w_m \approx 220$ nm, and it results in the maximum MD_G. Consequently, the relation of $w_{m,opt}$ to w_s shows that w_m should be chosen differently: $w_m \cong w_s$ for $w_s \leq 340$ nm and $w_m \approx 220$ nm for $w_s > 340$ nm. The relation between the maximum MD_G associated with $w_{m,opt}$ and w_s is shown in Fig. 3(b). As w_s increases up to 340 nm, the metal slot becomes wider, and the two peaks of $\Gamma(z)$ at the graphene positions are lowered. This leads to the decrease of the maximum MD_G. If w_s increases further above 340 nm, the confinement of the mode in the Si strip becomes substantial, and the peak $\Gamma(z)$ at the upper graphene position is lowered. Hence, the maximum MD_G keeps decreasing.

The relation of the IL_G to w_s, calculated with w_m set at $w_{m,opt}$, is shown in Fig. 3(c). Similar to the MD_G, the IL_G decreases as w_s increases up to 330 nm. However, it increases rapidly and seems to saturate as w_s increases further. When the chemical potential of graphene is ±0.6 eV, the absorption of 1550 nm light by graphene is very small. Hence, the IL_G is mainly determined by the absorption by the metal slot, which is small for a large value of w_m. Since $w_{m,opt}$ decreases rapidly to ∼220 nm for $w_s > 340$ nm, the IL_G becomes large. To choose an appropriate value of w_s, we considered the figure of merit for the GIMSA waveguide (FoM_G), which is defined as the ratio of the MD_G to the IL_G. The FoM_G is shown as a function of w_s in Fig. 3(c). The maximum FoM_G of 3.90 exists when $w_s = 330$ nm and $w_m = 324$ nm. In this case, the MD_G is 0.682 dB/μm, and the IL_w is 0.175 dB/μm. The waveguide in [26], which is structurally similar to the GIMSA waveguide, has a metal slot width of 200 nm and a Si strip width of 150 nm. Its modulation depth, insertion loss, and figure of merit are 0.316 dB/μm, 0.087 dB/μm, and 3.63, respectively; it has a smaller figure of merit than the GIMSA waveguide. In addition, as shown below, the smaller widths require a longer coupler connecting the waveguide to a Si photonic waveguide, which has a larger coupler loss. This is not considered in [26].

B. COMPREHENSIVE DESIGN OF THE EAM

The EAM should be designed to be as small and low-loss as possible. For this purpose, the taper region length (l_c) and taper end width (w_c) of the coupler should be well determined, and the GIMSA waveguide needs to be refined if necessary. To calculate the coupler loss, we simulated the modulator by using the finite difference time domain (FDTD) method (FDTD, Lumerical Inc.). Since the field profile of the GIMSA waveguide mode is hardly affected by the graphene

layers, for simplicity, we considered the GIMSA waveguide without the graphene layers. The coupler loss was obtained by subtracting the loss (in dB) of the GIMSA waveguide from the power loss (in dB) between the input and output Si photonic waveguides and dividing the subtraction result by 2. For a given value of w_s, we set w_m at $w_{m,opt}$ and determined the optimal value of l_c for which the coupler loss is minimized. The relations of the optimal length $l_{c,opt}$ to w_s are shown for a few values of w_c in Fig. 4(a), and those of the coupler loss associated with $l_{c,opt}$ to w_s are shown in Fig. 4(b). Since w_m increases as w_s increases up to 340 nm, both $l_{c,opt}$ and the coupler loss decrease. Then, they increase since w_m decreases as w_s increases further. Consequently, they become minimum at $w_s = 340$ nm near which the FoM_G is maximum. On the whole, $l_{c,opt}$ increases with w_c, but the coupler loss for $w_c = 500$ nm is smaller than those for $w_c = 450$ nm and 550 nm.

With the information gathered up to this point, the optimal values of w_s and w_c are determined as follows. In general, the extinction ratio of an intensity modulator used for short-reach data communications is a few dBs [4]. Hence, we determined the length of the GIMSA waveguide, l_G such that the extinction ratio obtained from it is 3 dB (*i.e.*, $l_G = 3/MD_G$). Then, the total length of the modulator, l_M is given by $l_G + 2l_{c,opt}$, and its total insertion loss IL_M is given by two times the coupler loss plus $l_G \times IL_G$. The calculated relations of l_M and the IL_M to w_s are shown for $w_c = 450$ nm, 500 nm, and 550 nm in Fig. 4(c). As w_s increases up to 340 nm, l_G increases by about a factor of two, but $l_{c,opt}$ decreases. Consequently, l_M slowly increases. For $w_s > 340$ nm, both l_G and $l_{c,opt}$ increase, and l_M rapidly increases. The curves for the IL_M are similar to those for the IL_G and the coupler loss. We defined the figure of merit for the modulator (FoM_M) as $1/(l_M \times IL_M)$, and the relations of the FoM_M to w_s are shown in Fig. 4(d). The FoM_M is maximum when w_s and w_c are 320 nm and 500 nm, respectively. Therefore, the determined values of w_s, w_m, w_c, l_c, and l_G are 320 nm, 316 nm, 500 nm, 1.05 μm, and 4.13 μm, respectively (in this case, the MD_G is 0.729 dB/μm, and the IL_G is 0.187 dB/μm). It is noteworthy that the value of w_s for the largest FoM_M is different from that for the largest FoM_G. The designed modulator has a length of 6.23 μm and an insertion loss of 1.01 dB. We simulated the designed modulator by using the FDTD method. The electric field distributions on the plane $z = 0$ nm are shown in Fig. 5. When the graphene chemical potential is 0.2 eV (*i.e.*, $\mu_{c1} = -\mu_{c2} = 0.2$ eV), the electric field becomes weak in the output Si strip waveguide. However, as shown in Fig. 5(b), it is slightly weakened while traversing the modulator when $\mu_{c1} = -\mu_{c2} = 0.6$ eV. There are periodic lobes of length ~350 nm in the GIMSA waveguide. They are attributed to the Fabry-Perot resonance caused by weak reflection from the couplers. The length agrees well with half a wavelength (1550 nm) divided by the effective index of the GIMSA waveguide mode (2.169).

Up to this point, it has been assumed that the graphene overlap width w_o and the rail width w_r are infinite. For the GIMSA waveguide with $w_s = 320$ nm, $w_m = 316$ nm, and $w_r = \infty$, we calculated the MD_G and the IL_G with respect to w_o. The MD_G and the IL_G are almost constant for $w_o \geq 500$ nm, because most of the electric field in the GIMSA waveguide is confined in the metal slot, and w_o is set at 500 nm. Then, we calculated them with respect to w_r under the assumption that the gap width w_g is infinite. If $w_r \geq 300$ nm, the MD_G and the IL_G are almost independent of w_r, and w_r is set at 300 nm. For $w_r = 300$ nm, the MD_G and the IL_G do not change depending on w_g.

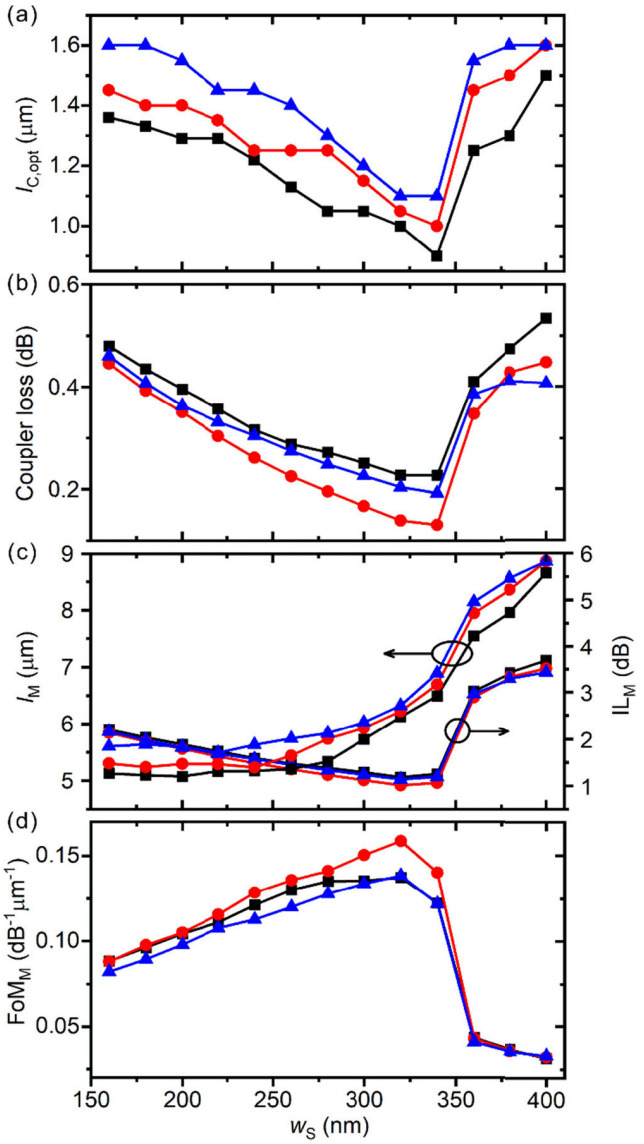

FIGURE 4. Characteristics of the coupler and the EAM at a wavelength of 1550 nm. (a) Relations of the optimal coupler length $l_{c,opt}$ to w_s. (b) Relations of the coupler loss, calculated for $l_c = l_{c,opt}$, to w_s. The relations in (a) and (b) were calculated for $w_m = w_{m,opt}$. (c) Relations of the total length l_M and total insertion loss (IL_M) of the EAM to w_s. The relations were calculated for $w_m = w_{m,opt}$ and $l_c = l_{c,opt}$. (d) Relations of the figure of merit of the modulator (FoM_M), defined as the inverse of the product of l_M and the IL_M, to w_s. The relations in all the panels were calculated for $w_c = 450$ nm (black square symbols), 500 nm (red circle symbols), and 550 nm (blue triangle symbols).

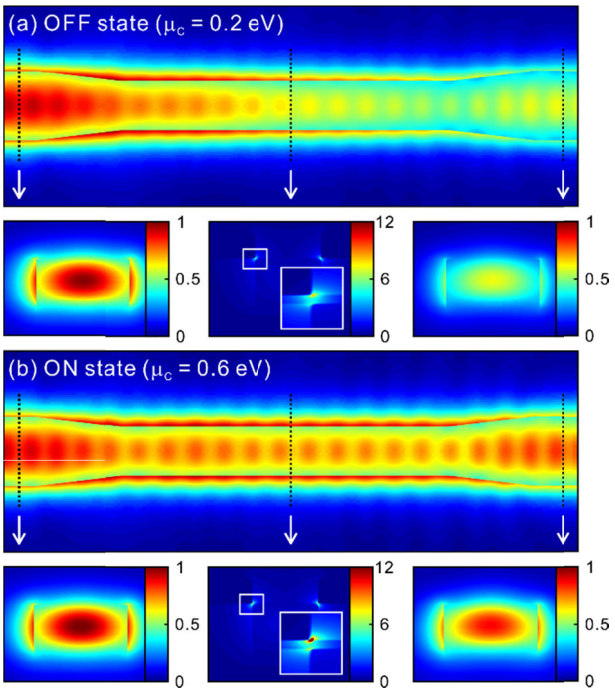

FIGURE 5. Electric field distributions in the designed EAM at $z = 0$ when the EAM is in (a) the on-state ($\mu_{c1} = -\mu_{c2} = 0.6$ eV) and (b) the off-state ($\mu_{c1} = -\mu_{c2} = 0.2$ eV). The cross-sectional distributions of |E| in the input Si photonic waveguide, the GIMSA waveguide, and the output Si photonic waveguide are shown. The distributions were calculated at a wavelength of 1550 nm.

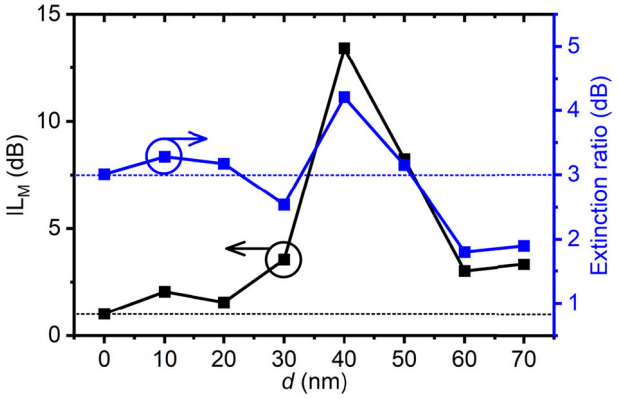

FIGURE 6. Dependence of the extinction ratio and IL_M of the designed EAM on the misalignment distance d between the metal slot and the Si strip.

During the fabrication of the EAM, there is a chance that the metal slot is not perfectly aligned to the Si strip. To determine the influence of this fabrication error, we used the FDTD method to simulate the EAM in which the metal slot is translated by a distance d in the y-direction from its ideal position. We calculated the on-state and off-state differences between the optical powers (in dB) carried by the input and output Si photonic waveguides. From the differences, we determined the extinction ratio and IL_M of the EAM with respect to d. As shown in Fig. 6, except the case of $d = 40$ nm, the extinction ratio and the IL_M do not change significantly from their ideal values while d increases up to 70 nm. In the case of $d = 40$ nm, the GIMSA waveguide mode is not well converted into the Si waveguide mode by the output coupler and reflected from the coupler. This may be because the GIMSA waveguide mode for $d = 40$ nm is almost antisymmetric and does not match the symmetric Si waveguide mode. Strictly saying, the tolerance of the alignment process is 30 nm, but an alignment error of 70 nm could be tolerated.

C. ELECTRIC CHARACTERISTICS OF THE EAM

Finally, it is necessary to analyze the 3-dB bandwidth and energy consumption of the EAM. To do so, the device capacitance and resistance of the EAM should be determined. They are affected by the spacing between electrode 1 and the metal rail (w_g). If w_g is small, the parasitic capacitance between electrode 1 and the metal rail is not negligible and affects the device capacitance. If w_g is large, the device resistance becomes large. We calculated the parasitic capacitance by using a commercial software (Device, Lumerical Inc.) and found that it becomes smaller than 0.27 fF for $w_g \geq 400$ nm and negligible compared to the device capacitance. The device capacitance C_d is determined by the parallel-plate capacitance between the graphene layers, C_g and the quantum capacitance of graphene, C_q. C_g is given by $\varepsilon_0\varepsilon_a l_G(w_r + w_o/2 + w_m/2)/t_a$, where ε_0 is the vacuum permittivity, $\varepsilon_a(= 10.3)$ is the dielectric constant of Al_2O_3, and t_a is the thickness of the Al_2O_3 layer. C_{q1} for the lower graphene and C_{q2} for the upper graphene are given by $2e^2\mu_c l_G w_i/[\pi(\hbar v_F)^2]$ for $i = 1$ and 2 [17], where e is the electron charge, $\hbar$ is the reduced Planck constant, and v_F is the Fermi velocity in graphene. $w_1 = w_r + w_o/2 + w_m/2$, and $w_2 = w_o$. C_g, C_{q1}, and C_{q2} are 26.6 fF, 0.275 pF, and 0.194 pF, respectively. C_d is given by $C_d = 1/(1/C_g + 1/C_{q1} + 1/C_{q2})$ and it is 21.6 fF. The device resistance R_d is given by $[2r_c + r_s(w_r + w_o + w_m + w_g)]/l_G$, where r_c and r_s represent the contact resistance and sheet resistance of graphene, respectively. If $r_c = 100\ \Omega \cdot \mu$m [28] and $r_s = 125\Omega$/sq [29], R_d is calculated to be 94.5 Ω. The 3-dB bandwidth f_{3dB} is given by $f_{3dB} = 1/(2\pi R_d C_d)$, which is calculated to be 78.1 GHz. The energy consumption E_b is given by $E_b = C_d(\Delta V_d)^2/4$ if the non-return-to-zero modulation format is used [30], [31]. ΔV_d is the difference between the driving voltages required to make μ_{c1} equal to 0.2 eV and 0.6 eV. ΔV_d can be calculated by using the expression for the driving voltage V_d in [32]. It is 4.93 V, and $E_b = 131$ fJ/bit. In many realized graphene-based devices, r_c and r_s are usually larger than the values used for the calculation. They mainly influence f_{3dB}, and f_{3dB} is reduced to 17.3 GHz if $r_c = 500\ \Omega \cdot \mu$m and $r_s = 500\ \Omega$/sq. Therefore, small r_c and r_s are essential for large f_{3dB}.

It would be valuable to compare our EAM with other theoretically investigated graphene-based EAMs. Many previous works focused on just graphene-based nanoplasmonic waveguides, not considering their integration into a Si photonics platform [15]–[17], [19]. Those waveguides have better EAM characteristics than the GIMSA waveguide. However, couplers required to connect them to Si photonic

TABLE 1. Comparison of our EAM and previous graphene-based EAMs embedded in Si photonic integrated circuits.

Ref.	l_M (μm)	IL_M (dB)	FoM_M ($dB^{-1}\mu m^{-1}$)	BW (GHz)	E_b (fJ/bit)	Min. feature size (nm)
[14]	8.48	2.73	0.0432	185	32.1	160
[20]	8.5	3.07	0.0383	400	145	40
[21]	5.57 (9.14)[a]	1.14 (1.46)	0.157 (0.075)	480	140	30
[22]	5.70 (10.8)	0.998 (2.06)	0.176 (0.045)	6.8	418	75
[32]	15.3	0.573	0.114	46.4	630	190
Ours	6.23	1.01	0.135	78.1	131	316

[a]The values in parentheses are estimated based on the information in [21] and [22] under the assumption that the EAMs in [21] and [22] use just two graphene layers.

waveguides may be long or have a large loss since they are quite different from Si photonic waveguides. Consequently, actual EAMs based on them and such couplers are likely to be longer or more lossy than our EAM. A few graphene-based EAMs which are embedded in Si photonic integrated circuits [14], [20]–[22], [32] are explicitly compared with our EAM. The total lengths (l_M), total insertion losses (IL_M), FoM_M's, and 3-dB bandwidths of the EAMs are compared in Table 1. In addition, the minimum feature sizes required for the realization of the EAMs are compared. The EAMs in [21] and [22] use four and eight graphene layers, respectively. To our knowledge, there is no realized waveguide modulator using more than two graphene layers. To consider their realizability and compare them fairly with the other EAMs, l_M, the IL_M, and the FoM_M are estimated based on the information in [21] and [22] under the assumption that just two graphene layers are used for the EAMs. The estimated values are given in parentheses. Among the EAMs in Table 1, our EAM has the smallest value of l_M, a moderate value of the IL_M, and the largest value of the FoM_M when the estimated values are considered. Moreover, the minimum feature size of our EAM is largest. These are the advantages of our EAM compared to the previous EAMs. Therefore, our EAM looks promising as a compact low-loss modulator which can be relatively easily realized and well embedded in Si photonic integrated circuits.

IV. CONCLUSION

We have investigated the GIMSA waveguide for the purpose of developing a waveguide which has strong light-graphene interaction enhanced by a metal slot, can be realized by using 248 nm optical lithography, and can be efficiently connected to Si waveguides. We have demonstrated that the metal slot of the GIMSA waveguide is much wider than those used for the previous graphene-based waveguide modulators. This is contradictory to the common belief that narrower metal slots are preferred for stronger light-graphene interaction; this reduces the burden of fabricating narrow metal slots. We have also studied the GIMSA waveguide-based EAM which has the best performance as compared to the previous graphene-based EAMs. The investigated EAM is 6.23 μm long and has an extinction ratio of 3 dB and an insertion loss of 1.01 dB. The EAM may be realized by using a Si waveguide fabrication process, a graphene transfer process, and a liftoff process. The realization requires the alignment between the Si strip and the metal slot to be done precisely with an alignment error less than 30 nm. The EAM is highly likely to be practically merged into Si photonic integrated circuits as a compact low-loss modulator.

REFERENCES

[1] F. Bonaccorso, Z. Sun, T. Hasan, and A. C. Ferrari, "Graphene photonics and optoelectronics," *Nature Photon.*, vol. 4, no. 9, pp. 611–622, Aug. 2010.

[2] Q. Bao and K. P. Loh, "Graphene photonics, plasmonics, and broadband optoelectronic devices," *ACS Nano*, vol. 6, no. 5, pp. 3677–3694, May 2012.

[3] D. Akinwande, C. Huyghebaert, C.-H. Wang, M. I. Serna, S. Goossens, L.-J. Li, H.-S. P. Wong, and F. H. L. Koppens, "Graphene and two-dimensional materials for silicon technology," *Nature*, vol. 573, pp. 507–518, Sep. 2019.

[4] M. Romagnoli, V. Sorianello, M. Midrio, F. H. L. Koppens, C. Huyghebaert, D. Neumaier, P. Galli, W. Templ, A. D'Errico, and A. C. Ferrari, "Graphene-based integrated photonics for next-generation datacom and telecom," *Nature Rev. Mater.*, vol. 3, no. 10, pp. 392–414, Oct. 2018.

[5] M. Liu, X. Yin, and X. Zhang, "Double-layer graphene optical modulator," *Nano Lett.*, vol. 12, no. 3, pp. 1482–1485, Feb. 2012.

[6] C. T. Phare, Y.-H. Daniel Lee, J. Cardenas, and M. Lipson, "Graphene electro-optic modulator with 30 GHz bandwidth," *Nature Photon.*, vol. 9, no. 8, pp. 511–514, Aug. 2015.

[7] Y. Hu, M. Pantouvaki, J. Van Campenhout, S. Brems, I. Asselberghs, C. Huyghebaert, P. Absil, and D. Van Thourhout, "Broadband 10 Gb/s operation of graphene electro-absorption modulator on silicon," *Laser Photon. Rev.*, vol. 10, no. 2, pp. 307–316, Mar. 2016.

[8] H. Dalir, Y. Xia, Y. Wang, and X. Zhang, "Athermal broadband graphene optical modulator with 35 GHz speed," *ACS Photon.*, vol. 3, no. 9, pp. 1564–1568, Sep. 2016.

[9] J. Wang, Z. Cheng, Z. Chen, X. Wan, B. Zhu, H. K. Tsang, C. Shu, and J. Xu, "High-responsivity graphene-on-silicon slot waveguide photodetectors," *Nanoscale*, vol. 8, no. 27, pp. 13206–13211, 2016.

[10] L. Abdollahi Shiramin, W. Xie, B. Snyder, P. De Heyn, P. Verheyen, G. Roelkens, and D. Van Thourhout, "High extinction ratio hybrid graphene-silicon photonic crystal switch," *IEEE Photon. Technol. Lett.*, vol. 30, no. 2, pp. 157–160, Jan. 15, 2018.

[11] Z. Cheng, X. Zhu, M. Galili, L. H. Frandsen, H. Hu, S. Xiao, J. Dong, Y. Ding, L. K. Oxenløwe, and X. Zhang, "Double-layer graphene on photonic crystal waveguide electro-absorption modulator with 12 GHz bandwidth," *Nanophotonics*, vol. 9, no. 8, pp. 2377–2385, Nov. 2019.

[12] D. Ansell, I. P. Radko, Z. Han, F. J. Rodriguez, S. I. Bozhevolnyi, and A. N. Grigorenko, "Hybrid graphene plasmonic waveguide modulators," *Nature Commun.*, vol. 6, no. 1, p. 8846, Nov. 2015.

[13] R. Hao, J. Jiao, X. Peng, Z. Zhen, R. Dagarbek, Y. Zou, and E. Yi, "Experimental demonstration of a graphene-based hybrid plasmonic modulator," *Opt. Lett.*, vol. 44, no. 10, pp. 2586–2589, May 2019.

[14] Y. Kim and M.-S. Kwon, "Solid-electrolyte-gated graphene-covered metal-insulator-silicon-insulator-metal waveguide with a remarkably large modulation depth," *IEEE Access*, vol. 7, pp. 174312–174324, 2019.

[15] R. Hao, Z. Ye, X. Peng, Y. Gu, J. Jiao, H. Zhu, W. E. I. Sha, and E. Li, "Highly efficient graphene-based optical modulator with edge plasmonic effect," *IEEE Photon. J.*, vol. 10, no. 3, pp. 1–7, Jun. 2018.

[16] R. Hao, Z. Ye, Y. Gu, X. Peng, H. Chen, and E. Li, "Large modulation capacity in graphene-based slot modulators by enhanced hybrid plasmonic effects," *Sci. Rep.*, vol. 8, no. 1, p. 16830, Nov. 2018.

[17] L. Ye, K. Sui, Y. Zhang, and Q. H. Liu, "Broadband optical waveguide modulators based on strongly coupled hybrid graphene and metal nanoribbons for near-infrared applications," *Nanoscale*, vol. 11, no. 7, pp. 3229–3239, Feb. 2019.

[18] B. Wang, S. Blaize, J. Seok, S. Kim, H. Yang, and R. Salas-Montiel, "Plasmonic-based subwavelength Graphene-on-hBN modulator on silicon photonics," *IEEE J. Sel. Topics Quantum Electron.*, vol. 25, no. 3, pp. 1–6, May 2019.

[19] M. Su, B. Yang, J. Liu, H. Ye, X. Zhou, J. Xiao, Y. Li, S. Chen, and D. Fan, "Broadband graphene-on-silicon modulator with orthogonal hybrid plasmonic waveguides," *Nanophotonics*, vol. 9, no. 6, pp. 1529–1538, May 2020.
[20] B.-H. Huang, W.-B. Lu, X.-B. Li, J. Wang, and Z. Liu, "Waveguide-coupled hybrid plasmonic modulator based on graphene," *Appl. Opt.*, vol. 55, no. 21, pp. 5598–5602, Jul. 2016.
[21] X. Peng, R. Hao, Z. Ye, P. Qin, W. Chen, H. Chen, X. Jin, D. Yang, and E. Li, "Highly efficient graphene-on-gap modulator by employing the hybrid plasmonic effect," *Opt. Lett.*, vol. 42, no. 9, pp. 1736–1739, Apr. 2017.
[22] Z. Wu and Y. Xu, "Design of a graphene-based dual-slot hybrid plasmonic electro-absorption modulator with high-modulation efficiency and broad optical bandwidth for on-chip communication," *Appl. Opt.*, vol. 57, no. 12, pp. 3260–3267, Apr. 2018.
[23] Z. Ma, M. H. Tahersima, S. Khan, and V. J. Sorger, "Two-dimensional material-based mode confinement engineering in electro-optic modulators," *IEEE J. Sel. Topics Quantum Electron.*, vol. 23, no. 1, pp. 81–88, Jan. 2017.
[24] Y. Ding, X. Guan, X. Zhu, H. Hu, S. I. Bozhevolnyi, L. K. Oxenløwe, K. J. Jin, N. A. Mortensen, and S. Xiao, "Efficient electro-optic modulation in low-loss graphene-plasmonic slot waveguides," *Nanoscale*, vol. 9, no. 40, pp. 15576–15581, 2017.
[25] M. Ono, M. Hata, M. Tsunekawa, K. Nozaki, H. Sumikura, H. Chiba, and M. Notomi, "Ultrafast and energy-efficient all-optical switching with graphene-loaded deep-subwavelength plasmonic waveguides," *Nature Photon.*, vol. 14, no. 1, pp. 37–43, Jan. 2020.
[26] Y. Zhu, C. Deng, L. Huang, G. Hu, B. Yun, R. Zhang, and Y. Cui, "Hybrid plasmonic graphene modulator with buried silicon waveguide," *Opt. Commun.*, vol. 456, Feb. 2020, Art. no. 124559.
[27] G. W. Hanson, "Dyadic Green's functions and guided surface waves for a surface conductivity model of graphene," *J. Appl. Phys.*, vol. 103, no. 6, Mar. 2008, Art. no. 064302.
[28] J. S. Moon, M. Antcliffe, H. C. Seo, D. Curtis, S. Lin, A. Schmitz, I. Milosavljevic, A. A. Kiselev, R. S. Ross, D. K. Gaskill, P. M. Campbell, R. C. Fitch, K.-M. Lee, and P. Asbeck, "Ultra-low resistance ohmic contacts in graphene field effect transistors," *Appl. Phys. Lett.*, vol. 100, no. 20, May 2012, Art. no. 203512.
[29] S. Bae, H. Kim, Y. Lee, X. Xu, J.-S. Park, Y. Zheng, J. Balakrishnan, T. Lei, H. Ri Kim, Y. I. Song, Y.-J. Kim, K. S. Kim, B. Özyilmaz, J.-H. Ahn, B. H. Hong, and S. Iijima, "Roll-to-roll production of 30-inch graphene films for transparent electrodes," *Nature Nanotechnol.*, vol. 5, no. 8, pp. 574–578, Jun. 2010.
[30] S. J. Koester, H. Li, and M. Li, "Switching energy limits of waveguide-coupled graphene-on-graphene optical modulators," *Opt. Express*, vol. 20, no. 18, pp. 20330–20341, Aug. 2012.
[31] D. A. B. Miller, "Energy consumption in optical modulators for interconnects," *Opt. Express*, vol. 20, no. S2, pp. A293–A308, Mar. 2012.
[32] Y. Kim and M.-S. Kwon, "Electroabsorption modulator based on inverted-rib-type silicon waveguide including double graphene layers," *J. Opt.*, vol. 19, no. 4, Mar. 2017, Art. no. 045804.

JIHOON SEO received the B.S. degree in electrical engineering from the Ulsan National Institute of Science and Technology (UNIST), Ulsan, South Korea, in 2019, where he is currently pursuing the Ph.D. degree.

MIN-SUK KWON received the B.S. (summa cum laude), M.S., and Ph.D. degrees in electrical engineering from the Korea Advanced Institute of Science and Technology (KAIST), Daejeon, South Korea, in 1998, 2000, and 2005, respectively. He was a Postdoctoral Research Associate with KAIST and the University of Southern California. He joined the Department of Optical Engineering, Sejong University, as a full-time Lecturer, in September 2007. From March 2009 to January 2012, he was an Assistant Professor. Since January 2012, he has been working as an Associate Professor with the Department of Electrical Engineering, Ulsan National Institute of Science and Technology (UNIST). His research interests include thermo-optically induced long-period gratings, integrated-optical sensors-based on micro-ring resonators, long-period waveguide gratings, surface plasmon polaritons, development of nanoplasmonic waveguide devices, and graphene-based waveguide devices.